Clinical, radiological, and genetic characteristics of 16 patients with ACO2 gene defects: Delineation of an emerging neurometabolic syndrome

SPi	Journal Code	Article ID	Dispatch: 03-JAN-19	CE: Jenifer
	JIMD	12022	No. of Pages: 12	ME:

Received: 25 September 2018 | Accepted: 7 December 2018

DOI: 10.1002/jimd.12022

WILEY JIMD SSIEM

ORIGINAL ARTICLE

Clinical, radiological, and genetic characteristics of 16 patients with *ACO2* gene defects: Delineation of an emerging neurometabolic syndrome

Rajech Sharkia[1,2] | Klaas J. Wierenga[3] | Amit Kessel[4] | Abdussalam Azem[4] | Enrico Bertini[5] | Rosalba Carrozzo[5] | Alessandra Torraco[5] | Paola Goffrini[6] | Camilla C. Berti[6] | Eileen M. McCormick[7] | Barbara Plecko[8,9] | Andrea Klein[10] | Lucia Abela[11] | Holger Hengel[12,13] | Ludger Schöls[12,13] | Stavit Shalev[14,15] | Morad Khayat[15] | Muhammad Mahajnah[14,16] | Ronen Spiegel[14,17]

[1]The Triangle Regional Research and Development Center, Kafr Qari, Israel

[2]Beit-Berl Academic College, Beit-Berl, Israel

[3]Department of Pediatrics, ~~Division of Genetics~~, Oklahoma City, ~~Oklahoma~~

[4]Department of Biochemistry and Molecular Biology, Faculty of Life Sciences, Tel-Aviv University, Tel-Aviv, Israel

[5]Unit of Muscular and Neurodegenerative Disorders, Laboratory of Molecular Medicine, Bambino Gesu' Children's Research Hospital, Rome, Italy

[6]Department of Chemistry, Life Sciences and Environmental Sustainability, University of Parma, Parma, Italy

[7]Department of Pediatrics, Oakland University William Beaumont School of Medicine, Rochester, Michigan

[8]Division of Child Neurology, University Children's Hospital Zurich, Zurich, Switzerland

[9]Department of Pediatrics, Medical University Graz, Graz, Austria

[10]Department of Pediatric Neurology, University Children's Hospital Basel and University Children's Hospital, Bern, Switzerland

[11]Molecular Neurosciences, Developmental Neuroscience, UCL Institute of Child Health, London, UK

[12]German Research Center for Neurodegenerative Diseases (DZNE), Tübingen, Germany

[13]Department of Neurodegenerative Diseases and Hertie-Institute for Clinical Brain Research, University of Tübingen, Tübingen, Germany

[14]Rappaport Faculty of Medicine, Technion- Israel Institute of Technology, Haifa, Israel

[15]Genetic Institute, Emek Medical Center, Afula, Israel

[16]Child Neurology and Development Center, Hillel-Yaffe Medical Center, Hadera, Israel

[17]Pediatric Department B, Emek Medical Center, Afula, Israel

Correspondence
Ronen Spiegel, Department of Pediatrics B, Emek Medical Center, Afula 1834111, Israel.
Email: spiegelr@zahav.net.il; spiegel_ro@clalit.org.il

Funding information
DFG, Grant/Award Number: SCHO 754/5-2; telethon foundation, Grant/Award Number: GGP15041; Telethon Foundation, Italy, Grant/Award Number: GGP15041

Abstract

Mitochondrial aconitase is the second enzyme in the tricarboxylic acid (TCA) cycle catalyzing the interconversion of citrate into isocitrate and encoded by the nuclear gene *ACO2*. A homozygous pathogenic variant in the *ACO2* gene was initially described in 2012 resulting in a novel disorder termed "infantile cerebellar retinal degeneration" (ICRD, OMIM#614559). Subsequently, additional studies reported patients with pathogenic *ACO2* variants, further expanding the genetic and clinical spectrum of this disorder to include milder and later onset manifestations. Here, we report an international multicenter cohort of 16 patients (of whom 7 are newly diagnosed) with biallelic pathogenic variants in *ACO2* gene. Most patients present in

early infancy with severe truncal hypotonia, truncal ataxia, variable seizures, evolving microcephaly, and ophthalmological abnormalities of which the most dominant are esotropia and optic atrophy with later development of retinal dystrophy. Most patients remain nonambulatory and do no acquire any language, but a subgroup of patients share a more favorable course. Brain magnetic resonance imaging (MRI) is typically normal within the first months but global atrophy gradually develops affecting predominantly the cerebellum. Ten of our patients were homozygous to the previously reported c.336C>G founder mutation while the other six patients were all compound heterozygotes displaying 10 novel mutations of whom 2 were nonsense predicting a deleterious effect on enzyme function. Structural protein modeling predicted significant impairment in aconitase substrate binding in the additional missense mutations. This study provides the most extensive cohort of patients and further delineates the clinical, radiological, biochemical, and molecular features of *ACO2* deficiency.

KEYWORDS

ACO2 gene, aconitase, infantile cerebellar retinal degeneration (ICRD), optic atrophy, neurodegenerative disorder, tricarboxylic acid cycle

1 | INTRODUCTION

The tricarboxylic acid (TCA) cycle also termed Krebs cycle is a vital energetic pathway located in the mitochondrial matrix. Genetic defects associated with human pathologies were described in most of the TCA enzymes usually leading to early onset encephalopathies.[1,2] The mitochondrial enzyme aconitate hydratase encoded by the nuclear gene *ACO2* (OMIM #100850) is the second enzyme in the TCA cycle (EC 4.2.1.3) and it catalyzes the stereo-specific isomerization of citrate into isocitrate.[3] In 2012, a deleterious homozygous mutation c.336C>G (p.Ser112Arg) in the *ACO2* gene was initially reported to result in a neurodegenerative disorder termed "infantile cerebellar retinal degeneration" (ICRD, OMIM #614559).[4] That report described eight affected individuals from two separate families who harbored the same homozygous mutation and presented with a distinct neurodegenerative phenotype characterized by infantile onset hypotonia, athetosis, inability to gain basic developmental milestones, convulsions, optic atrophy and retinal degeneration, culminating in early legal blindness and severe psychomotor handicap.[4]

Since then additional reports described less than a dozen additional *ACO2* deficient patients.[5–10] Interestingly, these reports further expanded the clinical spectrum of *ACO2* gene defects to include milder phenotypes such as isolated late onset optic atrophy recently termed optic atrophy 9 (OPA9, OMIM #616289). Here, we report seven new patients with biallelic mutations in the *ACO2* gene and in addition with the nine previously reported individuals we present the biggest clinical and genetic spectrum of this rare newly identified inborn error of metabolism.

2 | METHODS

2.1 | Patients

A cohort of 16 patients with confirmed molecular diagnosis of *ACO2* deficiency is included in the current study. Of these, seven are newly diagnosed and their presentation and clinical course are illustrated in detail (File S1). One of these patients (E1) has been previously published but with a focus on metabolomic biochemical findings.[11] In addition, we provide an update and follow-up on the clinical, radiological, and molecular details of the eight previously described patients.[4] Data were retrospectively collected from the physicians caring for these patients. This descriptive noninterventional multicenter study was approved by the Emek Medical Center Ethics Committee.

2.2 | Genetic analysis

Patients I1 to I8 were previously found to harbor the homozygous pathogenic mutation c.336C>G (p.Ser112Arg) in the *ACO2* gene.[4] Patients I9 and I10 (two siblings) and patients E2 and E3 (two additional siblings) were diagnosed by whole-exome sequencing (WES) performed on a research basis. Patient E1 was previously reported and the genetic diagnosis was made by WES performed on a research project on epileptic encephalopathies.[11] In patients A1, A2, and

A3 clinical WES was part of the clinical diagnostic evaluation and was performed by the Baylor Miraca Whole Genome Genetics Laboratory (patient A1), Ambry Genetics (patient A2), Gene Dx DNA diagnostic Experts (patient A3). Suspected pathogenic variants identified by WES were validated by means of Sanger sequencing. Familial segregation was further confirmed by Sanger sequencing.

In silico predictions for nonsynonymous variants were performed by PolyPhen-2 (http://genetics.bwh.harvard.edu/pph2/) Mutation Taster[12] and ConSurf web server.[13,14] Since the crystal structure of the human aconitase (NP_001089.1) has not been solved yet we built its predicted structure by using pig aconitase (pdb entry 1b0j), which is 96.5% identical in sequence to the human enzyme, as a template. We then used the predicted structure of human aconitase to evaluate the structural effects of the suspected pathogenic variants. The structure was predicted using the homology-modeling software Modeller.[15] The MolProbity web-server[16] was used to optimize side chain orientations and to add hydrogen atoms to the structure.

2.3 | Yeast analyses

Strains and oligos used in this work are reported in Table S1. All experiments, except transformation, were performed in synthetic complete (SC) medium media (0.69% yeast nitrogen base without amino acids [Formedium, UK]) supplemented with 1 g/L drop-out mix according to Kaiser et al,[17] except amino acids and bases necessary to keep plasmids. Media were supplemented with various carbon sources as indicated (Carlo Erba Reagents, Milan, Italy) in liquid phase or after solidification with 20 g/L agar (Formedium). Growth was performed with constant shaking at 28°C or 37°C. Transformation with suitable recombinant plasmids was used to express ACO1 and aco1 protein variants. Additional details are reported in File S2.

3 | RESULTS

A total of 16 patients comprise the study group and their age ranged between 5 and 23 years. Ten of them are of Arab Israeli descent and are designated I1 to I10 accordingly. Three patients are from the United States and are designated A1 to A3 accordingly, three patients are European (one Swiss designated E1, two siblings from Italy designated E2 and E3 accordingly). The clinical features of our patient cohort are summarized in Table 1.

3.1 | Clinical description

A clinical description of the patients not reported previously[4] are detailed in the supplementary data accordingly (File S1). All patients were born following an uneventful pregnancy and delivery, and growth parameters at birth including birth weight and head circumference were normal. Typically, patients presented within the first year of life usually during the first months except for patient A2 who developed seizures immediately after birth. Of note, a subgroup of three patients including A1, E2, and E3 presented a relatively milder phenotype with later onset of symptoms and more preserved neurological functions.

Most patients initially presented with generalized hypotonia, truncal ataxia, strabismus, seizures, and progressive postnatal microcephaly. Optic atrophy developed gradually and was clearly evident in most patients by the age of 5 years. This was invariably followed by progressive retinal degeneration from as early as the first 2 years of life. The retinal degeneration was associated with abnormal retinal pigmentation on fundus examination often described as "salt and pepper" appearance, and further confirmed by electroencephalography (EEG) when studied (11/16 patients) with completely absent or critically diminished responses, finally resulting in legal blindness. Disease course was marked by severe failure to thrive due to generalized muscle wasting and severe to profound developmental delay within the first 2 years of life. Twelve of 16 patients became severely microcephalic with head circumference ranging between z-scores (−2 to −4 SD) typically by the end of the first or second year. Most patients did not acquire any language skills or independent walking. In general, truncal ataxia and dystonic hand movements were dominant within the first 3 years of life and gradually decreased concomitantly with further motor regression. Most of the patients preserved oral feeding and despite their major neurological impairment did not experience recurrent episodes of aspiration pneumonia. Only two patients required insertion of a gastric tube. Five of six individuals above the age of 10 years, developed severely debilitating kyphoscoliosis, all belonging to the Israeli cohort. Over time the patients developed contractures, mostly of the Achilles tendon. Tendon reflexes of all extremities were elicited normally during the first years of life. In the Israeli patients, all of whom homozygous for the c.336C>G mutation tendon reflexes gradually decreased after the first year of life. Seizures occurred in most patients (13/16) and should be considered a main feature of the syndrome. In the majority it started within the first 2 years of life and included various types such as myoclonic and polymyoclonic jerks, generalized tonic-clonic, tonic, and focal spasms. Notably, in two patients the first spasms occurred during febrile illness. EEG studies typically showed slow background consistent with generalized encephalopathy in addition to convulsive activity. In most patients the seizures were successfully controlled with conventional anticonvulsive drugs. However, in two patients (E1 and A2) seizures

TABLE 1 Clinical characteristics of *ACO2* deficient patients

Patient	IS-1[a]	IS-2[a]	IS-3[a]	IS-4[a]	IS-5[a]	IS-6[a]	IS-7[a]	IS-8[a]	IS-9	IS-10	A-1	A-2	A-3	E-1[b]	E-2	E-3
Ethnicity	Arab muslin	Arab muslin	Arab muslin	Arab muslin	Arab muslin	Arab muslin	Arab muslin	Arab muslin	Arab muslin	Arab muslin	Hispanic/ Caucasian	Caucasian	Caucasian	Caucasian	African/ Caucasian	African/ Caucasian
Gender	Male	Female	Female	Female	Male	Female	Female	Female	Female	Female	Female	Male	Male	Female	Male	Male
Family no.	1	1	1	1	1	2	2	2	3	3	4	5	6	7	8	8
Current age (y)	23	18	12	8	6	14	13	7	19	16	8	Died at age 14 y 2 mo	5	Died at age 3 y 10 mo	8	6
Initial manifestation (age at presentation)	H, A (5 mo)	H, A (6 mo)	H, A (2 mo)	H, E (4 mo)	H, E (3 mo)	H, S (3 mo)	H, A (5 mo)	A, E (5 mo)	H, A (3 mo)	H, S (4 mo)	H, A (7 mo)	S (first day)	S (3 wk)	E, H (3 mo)	E (2 mo)	1 y
Ataxia (age at onset)	5 mo	6 mo	2 mo	8 mo	6 mo	5 mo	5 mo	5 mo	3 mo	6 mo	7 mo	Absent 2	12 mo	Absent	1 y	1 y
Hypotonia (age at onset)	5 mo	6 mo	2 mo	4 mo	3 mo	3 mo	5 mo	6 mo	3 mo	4 mo	7 mo	2 mo	4 mo	3 mo	1 y	1 y
Seizures (age at onset)	18 mo	3 y	1 y	18 mo	No	9 mo	1 y	5 mo	No	4 mo	No	First day	7 mo	14 mo	1 y	18 mo
Optic atrophy	2 y	2 y	18 mo	9 mo	2.5 y	3 y	5 y	2.5 y	9 mo	7 mo	8 mo	10 mo	2 y	7 mo	No	No
Strabismus	6 mo	8 mo	8 mo	4 mo	3 mo	5 mo	6 mo	5 mo	6 mo	7 mo	2 y	3 mo	No	3 mo	2 mo	
Abnormal ERG (age at examination)	NE	4 y	1 y	1 y	4 y	2 y	1.5 y	1.5 y	2 y	NE	2.5 y	10 mo	7 mo	NE	No (7 y)	No (5 y)
Global DD/MR	Profound	Profound	Profound	Profound	Severe	Profound	Profound	Severe	Profound	Profound	Moderate to severe	Profound	Profound	Profound	Moderate	Moderate
FTT -age at onset	First year	First year	First year	First year	First year	First year	First year	First year	First year	First year	No	First year	First year	First year	No	No
Microcephaly-age of onset	First year	First year	First year	Second year	Second year	First year	Third year	Third year	First year	First year	No	No	First year	First year	No	No
SNHL (age at onset)	NE	No	Moderate (2.5 y)	Severe (1.5 y)	Severe (2 y)	NE	NE	No	Moderate (3 y)	NE	No	No	No	No	No	No
Scoliosis/kyphosis	Mild	Severe	No	No	No	Severe	Severe	No	Severe	Severe	Mild	Mild	No	No	No	No
Able to walk	No	No	No	No	No	No	No	No	No	No	With assistance	No	No	No	Yes	Yes
Acquire language	No	No	No	No	No	No	No	N	No	No	Few words	No	No	No	Yes but delayed	Yes but delayed
Initial MRI (age)	NE	Normal (11 mo)	Mild CerA	Mild CorA	Normal (in utero)	CorA, thin CC (7 mo)	CorA, DYS (16 mo)	Mild CorA and CerA (1 y)	Normal (6 mo)	NE	Mild DYS (1 y)	Mild DYS (1 y)	Hyperintense T2 WM subcortical signal (1 mo)	Bilateral mild hyperintensities in globus pallidus (7 mo). Mildly	Normal 2 y	Normal 2 y

TABLE 1 (Continued)

Patient	IS-1[a]	IS-2[a]	IS-3[a]	IS-4[a]	IS-5[a]	IS-6[a]	IS-7[a]	IS-8[a]	IS-9	IS-10	A-1	A-2	A-3	E-1[b]	E-2	E-3
														elevated lactate on MRS		
Last MRI	NE	CerA, CorA, DYS (12 y)	CerA, CorA, thin CC, DYS (4 y)	CerA, CorA, DYS, thin CC (2.5 y)	Mild CerA, moderate CorA, DYS (12 y)	NE	NE	NE	CerA, CorA, thin CC, DYS (3 y)	NE	Mild DYS (2 y)	CerA, CorA, DYS, thin CC (10 y)	Cer A, Cor A (2 y) Cer A, Cor A, brain stem atrophy, abnormal elevated lactate peak on MRS (3 y)	CerA, CorA, DYS, thin CC (3 y)	CerA 4 y	CerA 3y
Muscle biopsy		Normal OXPHOS activity	Normal OXPHOS activity	NE	NE	Normal OXPHOS activity	NE	NE	Normal OXPHOS activity	NE	NE	NE	Normal	Reduced complex I-III	NE	NE
ACO2 mutation	Hom c.336C>G	Hom c.336C>G	Hom c.336C>G	Hom c.336C>G	Hom c.336C>G	Hom c.336C>G	Hom c.336C>G	Hom c.336C>G	Hom c.336C>G	Hom c.336C>G	c.260C>T c.685-1 _685delinsAA	c.1181G>A c.1722G>A	c.172C>T c.590A>G	c.1859G>A c.2048G>T	c.1787A>G c.2050C>T	c. 1787A>G c.2050C>T
Amino acid changes	S112R	S112R	S112R	S112R	S112R	S112R	S112R	S112R	S112R	S112R	S87L V229M	G394E D574X	R58X N197S	G620D G683V	H596R R684W	H596R R684W

Abbreviations: A, ataxia; CC, corpus callosum; CerA, cerebellar atrophy; CorA, cortical atrophy; DYS, sysmyelination; E, eye abnormalities; FTT, failure to thrive; H, hypotonia; hom, homozygous; NE, not evaluated; OXPHOS, oxidative phosphorylation; S, seizures; SNHL, sensorineural hearing loss.

[a]Previously reported.[4]

[b]Previously reported.[11]

were intractable. Other manifestations attributed to *ACO2* deficiency but seen less commonly included sensorineural hearing loss (four patients) and pes cavus (eight patients). Two patients died prematurely at 3 years (E1) and 14 years (A2) both due to severe neurological complications directly attributed to their disease. Patients I1 and I2 both had one sibling who died prematurely in the second decade of life with a similar phenotype; however, their genotype was not determined since their death occurred several years before the identification of the causative familial *ACO2* mutation.

Despite the rather distinctive severe phenotype shared by all patients we were able to define a subgroup of three patients including A1 (p.Val229Met/ p.Ser87Leu), and siblings E2 and E3 (p.His596Arg/p.Arg684Try) who displayed a somewhat attenuated presentation. They acquired variable walking abilities (either assisted or even independent although impaired by their ataxia), limited language skills and improved development and growth.

The majority of patients had extensive metabolic investigations that were all normal including lactate in plasma and cerebrospinal fluid (CSF), ammonia in plasma, amino acids in plasma, CSF and urine, acylcarnitine profile, organic acids in urine, total plasma homocysteine, serum transferrin isoelectric focusing, liver transaminases, blood count, thyroid hormones, serum very long chain fatty acids, CSF biogenic amines, pterins and pipecolic acid. Muscle biopsy was obtained from six patients (Table 1). In general, light microscopy as well as immunohistochemistry staining and electron microscopy when performed were largely normal. Respiratory chain enzyme activities were normal in five patients and revealed reduced activity of complex I/III (NADH cytochrome c reductase) in only one patient (E1). As reported previously glutamate oxidation was performed in two patients and was slightly reduced.[4] Seven patients underwent metabolomics plasma analysis that revealed alterations in the citric acid cycle, providing a fingerprint profile of *ACO2* deficiency.[11]

3.2 | Neuroimaging

Brain magnetic resonance imaging (MRI) was performed in 15 of 16 affected individuals (Figure 1). In eight patients more than one scan was undertaken allowing better understanding of disease progression. When performed before the age of 1 year brain imaging was either normal or showed minimal cortical and/or cerebellar atrophy as well as mild thinning of the corpus callosum (Figure 1A,E,I,K). Noteworthy, in one patient (I5) fetal MRI was performed at 30th week gestation and was unremarkable. Typically, brain imaging progressively became pathologic during the second year of life with the gradual advancement of cortical atrophy, cerebellar atrophy, slow but obvious thinning of the corpus callosum (Figure 1B,F) and the new emergence of abnormal white matter signals consistent with dysmyelination (Figure 1D,H). Beyond the age of 2 years the predominant MRI feature seen in all patients was global cerebellar atrophy characterized by considerable loss of volume of both the vermis and the cerebellar hemispheres (Figure 1B,C,F,G, J,L). This cerebellar shrinkage is associated with progressive supra-tentorial cortical atrophy seen predominantly in the central regions and to a lesser extent in the periphery (Figure 1G,J). Notably, peri-ventricular white matter signal abnormalities typically became visible early in disease course but later remained relatively unchanged despite clinical disease progression (Figure 1D,H). MR spectroscopy (MRS) was performed in three patients. In one patient (I4) it showed normal lactate levels and in the other two patients (E1 and A3) it showed elevation of lactate peaks in the basal ganglia and peri-ventricular regions consistent with mitochondrial function impairment. Of note, head ultrasound examination performed during the first months of life was typically normal. Taken together, brain imaging is an important diagnostic tool and in combination with the typical clinical course should raise high suspicion of ICRD.

3.3 | Genetic analysis

All the patients in our study cohort were found to harbor biallelic pathogenic variants in the *ACO2* gene. The details of the identified *ACO2* variants and their locations at the gene and protein levels are summarized in Table 1 and Figure 2A. Since most of the *ACO2* changes identified were novel missense variants, and were relatively distant from the enzyme's catalytic site, we employed in silico evaluation to estimate the pathogenic effect of the identified variants. We first used the well-accepted web-based softwares Mutation Taster, Polyphen-2, and ConSurf web server for calculating the evolutionary conservation of the variants, and then we employed protein structural modeling of the mitochondrial aconitase enzyme. The results of these in silico tests including the predicted structural effect of the variant on protein function are detailed in Figures S1-S9 and supplementary data (File S3).

The two sisters I9 and I10 were homozygous to the previously reported c.336C>G pathogenic variant. Of note, although they are not related to the previously eight reported patients, they live in the same town from which patients I1 to I5 originated. This town comprising about 50 000 inhabitants and is known for its very high (around 45%) consanguinity rate[18] predicting a relatively high carrier rate for this mutation. Noteworthy, the c.336C>G mutation carrier rate in this town was calculated to be 1% not justifying a prenatal couple screening in this population (Spiegel et al[4] unpublished data).

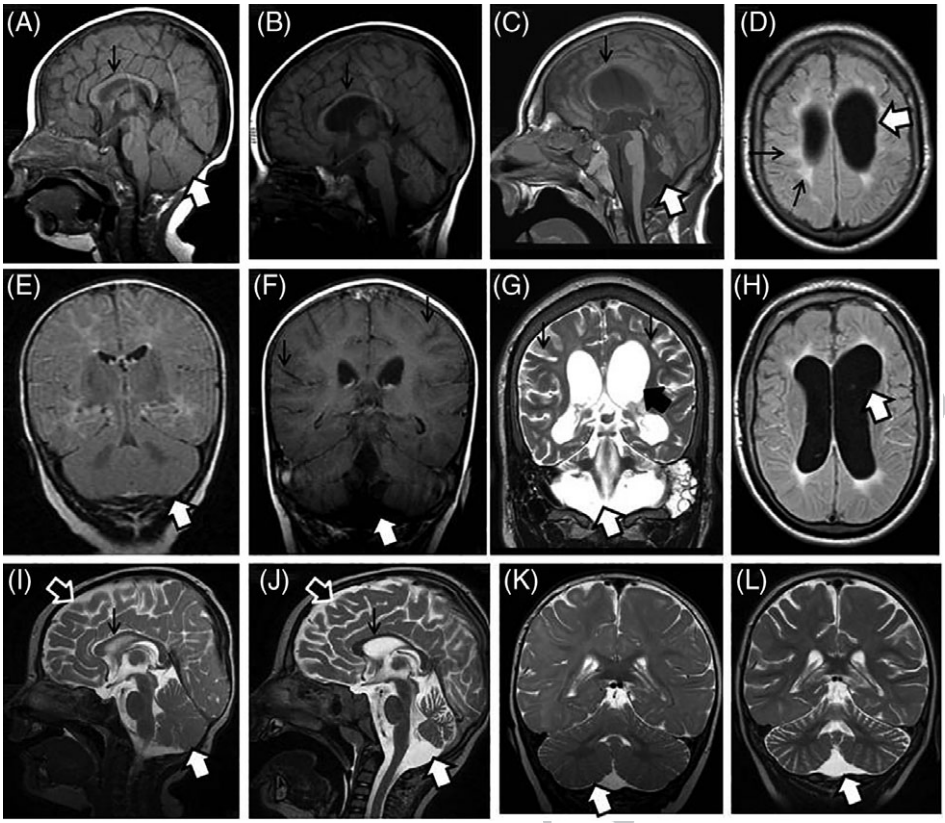

FIGURE 1 Typical MRI findings in *ACO2* deficient patients. A to H are serial images of patient A2. A and E were taken at the age of 7 months, B and F at the age of 3 years C, D, G, and H at the age of 11 years and 8 months. A-C: T1-weighted image at similar sagital section showing initially (A) normal cerebellum (thick white arrow) and corpus callosum (thin black arrow) with progressive thinning of corpus callosum (B, thin black arrow) and severely developing cerebellar atrophy (C, thick white arrow). E-G: Similar coronal sections of T1-weighted (E, F) and T2-weighted (G) scans showing initially normal cerebellum (E, white thick arrow) and cortex with later gradually evolving vermian and hemispheral cerebellar atrophy as demonstrated by enlarged folia and decreased cerebellar volume (F and G, white arrow). In addition, progressive cortical atrophy is evident both peripherally (F and G, thin black arrows) and centrally as evidenced by enlarged lateral ventricles (G, thick black arrow). D and H are T1-weighted at axial section showing significantly enlarged ventricles "pseudo hydrocephalus" as a result of considerable central cortical atrophy (thick white arrow) associated with abnormal peri-ventricular white matter signal consistent with dismyelination (D, thin black arrow). I to L are serial images of patient E1. I and K were taken at the age of 7 months and J and L at the age of 2 years and 8 months. I and J are T2 weighted similar sagittal images showing already thin corpus callosum (I, thin black arrow) mild cortical atrophy (I, thick black arrow) and very mild cerebellar atrophy (I, thick white arrow) at the age of 7 months with later almost disappearance of corpus callosum with only remnants of its posterior part (J, thin black arrow) and progressive cerebellar atrophy as evidenced by its volume loss (J, thick white arrow). K and L are T2 weighted similar coronal scans showing mainly progressive cerebellar atrophy (K and L, thick white arrows) with less prominent cortical atrophy

Patient A1 was found to be compound heterozygous for the predicted deleterious c.685-1_685delinsAA variant inherited from the mother resulting in the p.Val229Met predicting substantial enzyme conformational changes, and a nonsynonymous c.260C>T variant resulting in substitution of serine residue with leucine (p.Ser87Leu). The later variant, inherited from the father is predicted to reduce the binding of the enzyme to its substrate.

Patient A2 was compound heterozygous for the nonsense variant c.1722G>A predicting a premature truncation of the protein (p.Trp574*) and the missense variant c.1181G>A (p.Gly394Glu) predicting an interference and reduced substrate binding. Patient A3 is a compound heterozygous for the nonsense c.172C>T predicting an early premature truncation of the protein (p.Arg58*) and the missense variant c.590A>G (p.Asn197Ser) predicting disruption of both the catalytic activity and substrate binding.

Patient E1 was compound heterozygous for the nonsynonymous variants c.1859G>A (p.Gly620Asn) and the c.2048C>T (p.Gly683Val) both predicting interference with enzyme binding to its substrate. Patients E2 and E3 both harbored the two missense variants c.1787A>G (p.His596Arg) and c.2050C>T (p.Arg684Try) both are evolutionary conserved and are predicted to impair substrate binding.

3.4 | Functional studies in yeast

Since the sibling patients E2 and E3, who are both compound heterozygous for the missense variants His596Arg and Arg684Trp, displayed an attenuated phenotype we decided to investigate the functional consequences of these two variants in yeast by introducing the analogous amino acid substitutions in the *ACO1* gene, the *Saccharomyces cerevisiae ACO2* orthologue.[19] To evaluate the effect of each amino acid substitution, the oxidative growth, the oxygen consumption, and the aconitase activity were studied in the Δ*aco1* yeast strain carrying alone or in combination the two mutant alleles. As depicted in Figure S10, the strain containing the allele Arg681Trp does not show any respiratory defect while the one containing His593Arg allele displayed a significant oxidative growth defect (Figure S10A) and a reduction of oxygen consumption of 55% in respect to wild-type strain (Figure S10B). We then analyzed the effect of the variants on aconitase activity; the results, shown in Figure S10C, indicate that in both mutants the aconitase activity is affected being the values intermediate between the wild-type and the null mutant. In particular the aconitase activity is reduced in His593Arg mutant by 55% and by 25% in the Arg681Trp strain whereas in the null mutant the activity was almost completely abolished. These results clearly show that Arg681Trp is a mild variant compared with the more severe His593Arg variant.

In the presence of the two mutant alleles combined, both oxygen consumption and aconitase activity were significantly reduced when compared with those of the wild-type allele (Figure S10BII,CII) confirming that the phenotype observed in the strain carrying both His593Arg and Arg681Trp alleles was due to the compound hetero-allelic condition.

4 | DISCUSSION

In the current study, we further delineate the clinical and neuro-radiological phenotype of ICRD caused by biallelic *ACO2* pathogenic variants with an emphasis on disease major features and natural course. In addition we report of 10 novel *ACO2* variants and provide supporting data for their pathogenic role by means of structural protein modeling and functional yeast studies performed on two variants.

Accordingly, affected individuals typically present with a distinctive phenotype dominated by co-occurrence of infantile hypotonia, truncal ataxia, and evolving microcephaly, associated with ophthalmological abnormalities that include strabismus, nystagmus, gradual development of optic atrophy, and retinal degeneration. Generally, disease course in all affected individuals is progressive but we were able to differentiate between two subgroups: a severely deteriorating form advancing rapidly into a profound global psychomotor retardation state, where patients acquire no speech, become bedridden, and are legally blind already at late infancy, and an attenuated form where patients are still ambulatory with limited speech and communication skills and relatively preserved growth parameters.

Nevertheless, all the patients in our study display the major characteristics and therefore may be regarded within the phenotypic spectrum of ICRD. We speculate that severity may be correlated with residual enzyme activity. Unfortunately, we were unable to assay aconitase activity in most of our patients since this assessment is not readily available in a clinical setup but based on previous analyses performed in a research setup we speculate that enzyme activity of less than 20% of control is associated with classical ICRD phenotype.[4,8,9]

In support of this hypothesis we used yeast as model system to investigate functional consequences of the two missense variants (p.His596Arg and p.Arg684Trp), identified in patients E2 and E3 in compound heterozygosity exhibiting milder phenotype. Accordingly, both mutations showed reduced aconitase activity though to different extent; moreover when expressed in combination, mimicking the patient condition, enzyme activity determined in the yeast model was 60% of that of the wild-type control. Although this analysis is not equivalent to determination of enzyme activity in patient's cells (lymphoblasts or fibroblasts) it reflects decreased activity and furthermore mutation severity.

In agreement, Metodiev et al already showed in their study that partial decrease of 50% to 60% of control is associated with a milder phenotype of isolated adult optic atrophy (currently termed OPA9 OMIM# 616289) whereas a critical decrease of aconitase activity (5% of control) resulted in the most severe phenotype of lethal neonatal encephalopathy in two siblings thus suggesting a clear genotype phenotype correlation directly related to enzyme malfunction.[8] Recently, Marelli et al reported a 56 years' woman with mild cognitive delay and late, adult onset, progressive optic atrophy and spastic paraplegia due to biallelic *ACO2* mutations. Notably, aconitase enzyme activity measured in cultured fibroblasts was 50% of control further supporting clear correlation between clinical severity and enzyme activity.[7] Of interest, the clinical spectrum of *ACO2* gene defects was recently further extended to include early onset spastic paraplegia with sparing of cerebellar symptoms and optic atrophy.[5] In order to correlate residual enzyme activity with patients' phenotype and genotype we summarized all cases with biallelic *ACO2* mutations where aconitase activity was assessed (Table 2). Although preliminary, the table displays a clear correlation between residual enzyme activity and disease severity and age of onset. Accordingly, enzyme activity below 30% is associated with ICRD phenotype and enzyme

TABLE 2 Correlation of mitochondrial aconitase activity with clinical phenotype and genotype in patients with *ACO2* gene defects

Patient no.	1	2	3	4	5	6	7	8	9
Gender	Female	Male	Male	Male	Female	Male	Female	Male	Female
Current age	8 y	41 y	36 y	Died at 57 d	6 y	3 y	56 y	28 y	14 y
Ethnicity	Arab	French	French	Algerian	N.M	Afro-Caribbean and East Indian	N.M	Arab Bedouin	Arab Bedouin
Phenotype	ICRD	Isolated optic atrophy	Isolated optic atrophy	Neonatal epileptic encephalopathy	ICRD	ICRD	Late onset optic atrophy and progressive spastic paraplegia	Early onset progressive spastic paraparesis, microcepaly and ID	Early onset progressive spastic paraparesis, microcepaly and ID
Mutation	p.Ser112Arg/ p.Ser112Arg	p.Leu74Val/ p.Gly661Arg	p.Leu74Val/ p.Gly661Arg	p.Gly259Asp/ p.Gly259Asp/	p.Lys736Asn/ p.Lys776Asnfs*49	p.Pro712Leu/ p.Arg607Cys	p.Pro712Leu/ c.940+5G>C	p.Phe414Val/ p.Phe414Val	p.Phe414Val/p.Phe414Val
Enzyme activity (%)	12	58	66	5	31	20	50	~20	~20
Tissue examined	Lymphoblast	Fibroblast	Fibroblast	Fibroblast	Fibroblast	Fibroblast	Fibroblast	Lymphoblasts	Lymphoblasts
Reference	Spiegel et al[4] (current report IS-4)	Metodiev et al[8] (P1)	Metodiev et al[8] (P2)	Metodiev et al[8] (P3)	Metodiev et al[8] (P2)	Sadat et al[9]	Marelli et al[7]	Bouwkamp et al[5]	Bouwkamp et al[5]

Abbreviations: ICRD, infantile cerebellar and retinal dystrophy; ID, intellectual disability; N.M, not mentioned.

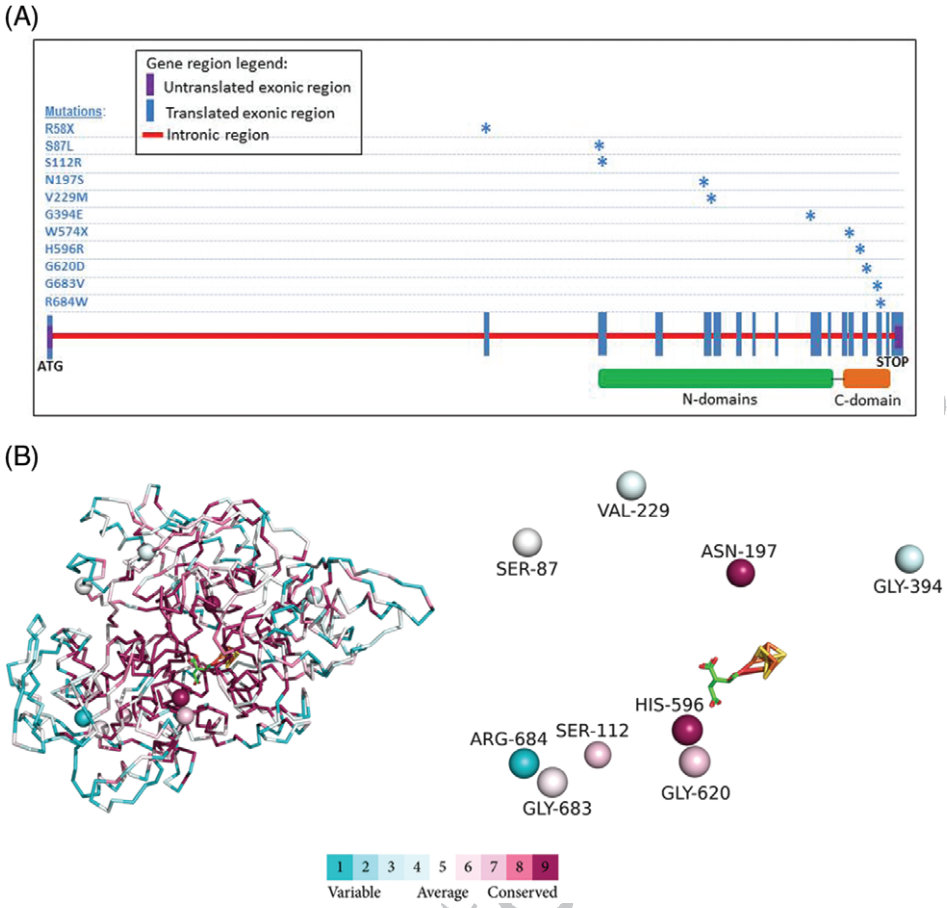

Color Figure - Print and Online

FIGURE 2 Schematic representation of exonic ACO2 and 3D structure of amino acid exchanges. A, Schematic representation of the localization of each of the mutants in relation with the exonic ACO2 protein. The amino acid was determined for all missense variants from the UCSC Genome Browser (genome.ucsc.edu). B, The location and evolutionary conservation of the ACO2 positions targeted by the missense mutations. The positions are shown as spheres. The left image shows the positions within the 3D structure of the enzyme, where the enzyme's backbone is shown as a ribbon, colored by evolutionary conservation. The conservation levels (cyan—lowest, maroon—highest; see color code in figure) were calculated by ConSurf (http://consurf.tau.ac.il)[13,14] using the Bayesian method. For clarity, the right image shows the locations of the isolated positions (conservation-colored spheres) with respect to the substrate, bound to the sulfur-iron complex (sticks). The separate representations of each *ACO2* missense mutation are shown in Figures S1-S9 and the structural analysis is described in File S2. In Figures S1-S9, α-helices are shown in red, β-strands in yellow, loops are in green, and hydrogen bonds are black-dashed lines. Suggested protein motions that may result from the mutations are shown as purple arrows, where straight arrows mark translations and curved arrows mark hinge motions. Only the relevant parts of the protein are shown, with respect to the bound substrate (isocitrate)

activities of 50% or higher are associated with late onset milder phenotypes such as isolated optic atrophy with or without progressive spastic paraparesis.

In the last two decades, MRI is becoming a major component in the diagnostic toolbox of patients with neurogenetic disorders. As expected, consecutive brain MR studies are also invaluable in the diagnostic evaluation of ICRD especially when combined with careful and strict assessment of the patients. Of note, MRI abnormalities appearance is delayed compared with the emergence of clinical symptoms. MR scans performed within the first year of life are typically normal or show mild abnormalities even when significant neurological impairment is already evident. Only later (usually within the second year of life) MR studies become pathologic with global cerebellar atrophy being the key component, associated with generalized cortical atrophy involving mainly the central regions with concomitant ventriculomegaly, thinning of the corpus callosum and peri-ventricular white matter signal abnormalities. This delay in brain imaging compared with clinical symptoms may frequently occur in other TCA defects[20] emphasizing the importance of repeating MRI studies as disease progress. MRS an emerging complementary study to conventional MRI, in particular when inborn errors of metabolism are clinically suspected, was performed in only three individuals in our cohort (A1, A3, E1). It showed abnormally elevated lactate peaks in two of the patients (A3, E1) which imply an underlying mitochondrial disorder. Taken together, abnormally elevated

lactate peaks in combination with cerebellar atrophy and typical clinical features including optic atrophy and retinal degeneration is highly suggestive of ICRD. We speculate that the increasing use of MRS in routine brain MR examinations particularly when a metabolic disorder is suspected will significantly contribute to the diagnostic rate of ICRD patients.

Except for the 10 Israeli patients originating from an inbred population all the other patients were compound heterozygous to apparently pathogenic variants. Interestingly about half of the mutations identified in our study were located within the small C-terminal domain (Figure 2A). Two nonsense mutations predicted a premature stop codon suggesting early truncation and thus loss of enzyme activity. The rest of the mutations were missense. According to our in silico structural modeling they are predicted to induce a negative effect on substrate binding (Figure S1-S9 and File S2). As expected all the variants, except for one (p.Ser87-Leu), are placed at evolutionary conserved amino acid and are predicted pathogenic by web-based prediction softwares (Mutation Taster and Polyphen-2).

Given the lack of informative metabolic biomarkers, the diagnosis of ICRD relies on meticulous and comprehensive clinical assessment of the patients in association with typical MRI findings. The diagnosis is then confirmed by demonstration of biallelic *ACO2* pathogenic variants. High throughput liquid chromatography-mass spectrometry (LC-MS) serum metabolomic analysis already shown to provide characteristic distinct fingerprint profile in ICRD patients,[11] and enzyme activity assay are currently available in research platforms but are expected to be available in clinical setup in the near future and will thus support/-confirm the diagnosis mainly in controversial or unequivocal cases.

In summary, ICRD is a rare neurodegenerative disorder, characterized by distinctive clinical phenotype and caused by deleterious mutations in the *ACO2* gene that severely disrupt the structure, thereby the function, of mitochondrial aconitase, a key enzyme in the TCA cycle.

ACKNOWLEDGMENTS

This work was supported in partially by the DFG trilateral project (Reference number SCHO 754/5-2). Yeast studies were performed with the support of Telethon Foundation, Italy grant GGP15041. We are grateful to the patients and their families for their cooperation. We also thank Metsada Pasmanik-Chor from the Bioinformatics Unit at the Faculty of Life Science, Tel Aviv University, for assessing the structure and mutations of ACO2 gene as appeared in Figure 2A.

CONFLICTS OF INTEREST

All the authors of this manuscript declare that they have no conflicts of interest.

Author contribution

R.S. and R.S. conceptualization of this study, drafting and editing of the manuscript, analysis and interpretation of data. A.K., A.A. acquisition and analysis of the structure modeling data and contributing to revising the manuscript. K.J.W. and M.M., acquisition and analysis the clinical and neuro-radiological data and contributing to revising the manuscript. H.H., L.S., P.G., M.K. and L.A. acquisition of the genetic data and contributing to revising the manuscript. E.B., E.M.M., B.P., A.K., R.C., A.T. and S.S. acquisition and analysis of the clinical data and contributing to revising the manuscript. P.G., and, C.C.B. acquisition and analysis of the functional yeast studies and contributing to revising the manuscript.

REFERENCES

1. Briere J, Favier J, Gimenez-Roqueplo AP, Rustin P. Tricarboxylic acid cycle dysfunction as a cause of human diseases and tumor formation. *Am J Phys Cell Phys*. 2006;291(6):C1114-C1120.
2. Rustin P, Bourgeron T, Parfait B, Chretien D, Munnich A, Rötig A. Inborn errors of the Krebs cycle: a group of unusual mitochondrial diseases in human. *Biochim Biophys Acta*. 1997;1361(2):185-197.
3. Beinert H, Kennedy MC. Aconitase, a two-faced protein: enzyme and iron regulatory factor. *FASEB J*. 1993;7(15):1442-1449.
4. Spiegel R, Pines O, Ta-Shma A, et al. Infantile cerebellar-retinal degeneration associated with a mutation in mitochondrial aconitase, ACO2. *Am J Hum Genet*. 2012;90(3):518-523.
5. Bouwkamp CG, Afawi Z, Fattal-Valevski A, et al. ACO2 homozygous missense mutation associated with complicated hereditary spastic paraplegia. *Neurol Genet*. 2018;4(2):e223.
6. Kelman JC, Kamien BA, Murray NC, Goel H, Fraser CL, Grigg JR. A sibling study of isolated optic neuropathy associated with novel variants in the ACO2 gene. *Ophthalmic Genet*. 2018;39(5):648-651.
7. Marelli C, Hamel C, Quiles M, et al. ACO2 mutations: a novel phenotype associating severe optic atrophy and spastic paraplegia. *Neurol Genet*. 2018;4(2):e225.
8. Metodiev MD, Gerber S, Hubert L, et al. Mutations in the tricarboxylic acid cycle enzyme, aconitase 2, cause either isolated or syndromic optic neuropathy with encephalopathy and cerebellar atrophy. *J Med Genet*. 2014;51:834-838.
9. Sadat R, Barca E, Masand R, et al. Functional cellular analyses reveal energy metabolism defect and mitochondrial DNA depletion in a case of mitochondrial aconitase deficiency. *Mol Genet Metab*. 2016;118(1):28-34.
10. Srivastava S, Gubbels CS, Dies K, Fulton A, Yu T, Sahin M. Increased survival and partly preserved cognition in a patient with ACO2-related disease secondary to a novel variant. *J Child Neurol*. 2017;32(9):840-845.

11. Abela L, Spiegel R, Crowther LM, et al. Plasma metabolomics reveals a diagnostic metabolic fingerprint for mitochondrial aconitase (ACO2) deficiency. *PLoS One*. 2017;12(5):e0176363.
12. Schwarz JM, Cooper DN, Schuelke M, Seelow D. MutationTaster2: mutation prediction for the deep-sequencing age. *Nat Methods*. 2014;11(4):361-362.
13. Ashkenazy H, Abadi S, Martz E, et al. ConSurf 2016: an improved methodology to estimate and visualize evolutionary conservation in macromolecules. *Nucleic Acids Res*. 2016;44(W1):344-350.
14. Glaser F, Pupko T, Paz I, et al. ConSurf: identification of functional regions in proteins by surface-mapping of phylogenetic information. *Bioinformatics*. 2003;19(1):163-164.
15. Sali A, Potterton L, Yuan F, van Vlijmen H, Karplus M. Evaluation of comparative protein modeling by MODELLER. *Proteins*. 1995;23(3):318-326.
16. Chen VB, Arendall WB, Headd JJ, et al. MolProbity: all-atom structure validation for macromolecular crystallography. *Acta Crystallogr D Biol Crystallogr*. 2010;66(1):12-21.
17. Kaiser C, Michaelis S, Mitchell A. *Methods in Yeast Genetics: A Cold Spring Harbor Laboratory Course Manual 1994 Edition*. Cold Spring Harbor Laboratory Press; 1994.
18. Sharkia R, Mahajnah M, Athamny E, Khatib M, Sheikh-Muhammad A, Zalan A. Changes in marriage patterns among the Arab community in Israel over a 60-year period. *J Biosoc Sci*. 2016;48(2):283-287.
19. Gangloff SP, Marguet D, Lauguin GJ. Molecular cloning of the yeast mitochondrial aconitase gene (*ACO1*) and evidence of a synergistic regulation of expression by glucose plus glutamate. *Mol Cell Biol*. 1990;10(7):3551-3561.
20. Carrozzo R, Verrigni D, Rasmussen M, et al. Succinate-CoA ligase deficiency due to mutations in SUCLA2 and SUCLG1: phenotype and genotype correlations in 71 patients. *J Inherit Metab Dis*. 2016;39(2):243-252.

SUPPORTING INFORMATION

Additional supporting information may be found online in the Supporting Information section at the end of the article.

How to cite this article: Sharkia R, Wierenga KJ, Kessel A, et al. Clinical, radiological, and genetic characteristics of 16 patients with *ACO2* gene defects: Delineation of an emerging neurometabolic syndrome. *J Inherit Metab Dis*. 2019;1–12. https://doi.org/10.1002/jimd.12022